ACS APPLIED MATERIALS & INTERFACES

Research Article

www.acsami.org

# Facile Synthesis of Novel Heterostructure Based on $SnO_2$ Nanorods Grown on Submicron Ni Walnut with Tunable Electromagnetic Wave Absorption Capabilities

Biao Zhao,[†] Bingbing Fan,[†] Gang Shao,*[,†] Wanyu Zhao,[†] and Rui Zhang*[,†,‡]

[†]School of Materials Science and Engineering, Zhengzhou University, Zhengzhou 450001, China

[‡]Zhengzhou Institute of Aeronautical Industry Management, Zhengzhou 450046, China

Supporting Information

**ABSTRACT:** In this work, the magnetic−dielectric core-shell heterostructure composites with the core of Ni submicron spheres and the shell of $SnO_2$ nanorods were prepared by a facile two-step route. The crystal structure and morphology were investigated by X-ray diffraction analysis, transmission electron microscopy (TEM), and field emission scanning electron microscopy (FESEM). FESEM and TEM measurements present that $SnO_2$ nanorods were perpendicularly grown on the surfaces of Ni spheres and the density of the $SnO_2$ nanorods could be tuned by simply varying the addition amount of $Sn^{2+}$ in this process. The morphology of Ni/$SnO_2$ composites were also determined by the concentration of hydrochloric acid and a plausible formation mechanism of $SnO_2$ nanorods-coated Ni spheres was proposed based on hydrochloric acid concentration dependent experiments. Ni/$SnO_2$ composites exhibit better thermal stability than pristine Ni spheres based on thermalgravimetric analysis (TGA). The measurement on the electromagnetic (EM) parameters indicates that $SnO_2$ nanorods can improve the impedance matching condition, which is beneficial for the improvement of electromagnetic wave absorption. When the coverage density of $SnO_2$ nanorod is in an optimum state (diameter of 10 nm and length of about 40−50 nm), the optimal reflection loss (RL) of electromagnetic wave is −45.0 dB at 13.9 GHz and the effective bandwidth (RL below −10 dB) could reach to 3.8 GHz (12.3−16.1 GHz) with the absorber thickness of only 1.8 mm. By changing the loading density of $SnO_2$ nanorods, the best microwave absorption state could be tuned at 1−18 GHz band. These results pave an efficient way for designing new types of high-performance electromagnetic wave absorbing materials.

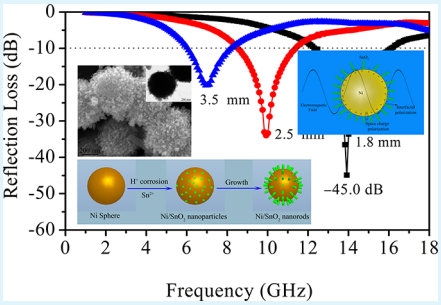


**KEYWORDS:** *Ni/$SnO_2$, core-shell, $SnO_2$ nanorods, electromagnetic wave absorption, dielectric loss, interfacial polarization*

## 1. INTRODUCTION

Heteronanostructure composites are an important class of materials, which not only derive the properties from their individuals but also probably pave the way to improve the functionality and multifunctional properties due to the interaction between individual constituents.[1−5] Recently, with the explosive development of electrical and electronic industries in gigahertz frequency, electromagnetic interference (EMI) from the invisible electromagnetic wave used in many fields continues to be a serious issue in society.[6−9] The unwanted electromagnetic wave cannot only interrupt electronic instruments but also be harmful to human beings.[10,11] Thus, to settle this invisible and omnipresent pollution, lots of effort has been devoted to exploiting a variety of materials and structures which can be applied as microwave absorbers for stealth or shielding unwanted electromagnetic waves.[12−15] They can absorb electromagnetic waves effectively and transform electromagnetic energy into heat energy or attenuate electromagnetic waves by interference.[16] There are numerous research papers about microwave absorbing materials in the X-band (8.2−12.4 GHz) with its application in military correspondence satellites, aviation authority, and defense tracking and Ku band (12.5−18 GHz) with its utilization in high-determination imaging radars, broadcast services, and satellite digital data transmission.[17,18] It is well-known that the electromagnetic wave absorption properties are crucially controlled by the relative complex permittivity ($\varepsilon_r = \varepsilon' - j\varepsilon''$) and permeability ($\mu_r = \mu' - j\mu''$) of absorbing materials.[19,20] The balance of the permittivity and permeability, called the electromagnetic wave impedance matching, is beneficial for the improvement of microwave attenuation.[21] According to loss mechanism of microwave energy, microwave absorbing materials could be clarified into two kinds: dielectric loss and magnetic loss.[12,22] An effective way to reach the impedance matching is to combine magnetic and dielectric materials, which are expected to achieve the excellent microwave absorption because of the cooperative effect on dissipation of electromagnetic wave energy.[21,23]

In the recent period, there is plentiful research in building composites based on Ni because of high permeability and easy preparation, which show the potential applications in electro-

Received: June 19, 2015
Accepted: August 10, 2015
Published: August 10, 2015





DOI: 10.1021/acsami.5b05482
ACS Appl. Mater. Interfaces 2015, 7, 18815−18823

magnetic wave absorption application.[24−36] Tong et al.[24] synthesized rambutan-like composites composed of Ni microspheres and oriented multiwall carbon nanotubes (MWCNTS). This heterostructures coated by short MWCNTs exhibited the minimal reflection loss of −37.9 dB occurring at 12.8 GHz. Wang et al.[26] prepared flower-like Ni/ZnO through an atomic layer deposition (ALD) method. The ZnO@Ni composite exhibits remarkably enhanced electromagnetic wave absorption properties compared to the pure ZnO. Xu and co-workers[27] fabricated the core-shell structured Ni/Polypyrrole composites with enhanced electromagnetic wave absorption. The enhanced electromagnetic absorption of composites is attributed to electromagnetic impedance matching due to the synergetic consequence of Ni cores and polypyrrole shells. In our previous report,[28] we designed core-shell composites composed of Ni cores and $Al_2O_3$ nanoflake shells and investigated electromagnetic wave absorption properties. From these results, it can force us to conclude that the electromagnetic wave absorption properties of Ni-based heterostructure composites can be significantly improved compared with the individual composition, which is assigned to proper impedance originating from combination of dielectric loss and magnetic loss.

As far as we know, there are few reports about the electromagnetic properties of Ni/$SnO_2$ heterostructure composites.[29,37] In the earlier literature,[37] $SnO_2$ nanoparticles coated Ni microspheres were successfully synthesized and their microwave properties were also investigated. However, the size of Ni particles is too large, which is close to the skin depth of metal Ni (∼1.0 $\mu$m), and the core-shell structure is ambiguously observed, which is harmful for interfacial polarization. In this work, the novel heterostructure of $SnO_2$ nanorods grown on a Ni submicron sphere was synthesized by a simple two-step method. The diameter and length of $SnO_2$ nanorods can be effectively controlled by tuning the amounts of Sn resource, which is critical for determining their microwave absorption properties.

## 2. EXPERIMENTAL SECTION

**2.1. Materials.** All chemicals used in this process are commercially available without further purification. Nickel chloride hexahydrate ($NiCl_2·6H_2O$), glycerol, trisodium citrate dehydrate, and sodium acetate were supplied by Xilong Chemical Reagent Co. Ltd. (Guangdong, China). $NaH_2PO_2·H_2O$ was supplied by Kemiou Chemical Reagent Co. Ltd. (Tianjin, China). Anhydrous ethanol, hydrochloric acid, and $SnCl_2·2H_2O$ were provided from Guangfu Chemical Reagent Technologies Co. Ltd. (Tianjin, China).

**2.2. Synthesis of Walnut-Like Ni Particles.** The Ni walnut spheres were synthesized according to our earlier literature.[34] In brief, $NiCl_2·6H_2O$ (1.2 g), sodium acetate (3.0 g), and trisodium citrate dihydrate (0.2 g) were dissolved in the mixture solution containing glycerol (30 mL) and distilled water (30 mL). Subsequently, 1.6 g of NaOH and sodium hypophosphite ($NaH_2PO_2·H_2O$, 3.2 g) were in turn introduced into the above mixture. The solution was transferred into an autoclave. The autoclave was heated to 140 °C and kept for 15 h. The final products were collected from the solution.

**2.3. Preparation of $SnO_2$ Nanorods Grown on Ni Particles.** The resultant walnut-like Ni spheres were dispersed in the mixture of 40 mL of distilled water and 20 mL of anhydrous ethanol. Then $SnCl_2·2H_2O$ (1 mmol) and hydrochloric acid (4 mL, 0.1 M) were added into the above solution. Then the mixture was shifted into an autoclave and heated to 200 °C for 15 h. The final product was filtered out and rinsed with anhydrous ethanol and distilled water three times. To investigate the influences of the concentration of hydrochloric acid and $SnCl_2·2H_2O$ on the morphologies of Ni/$SnO_2$ hybrids, a series of comparison experiments were performed. For convenience, the Ni/$SnO_2$ composites were prepared at 0.5, 1.0, 1.5, and 2.0 mmol of $SnCl_2·2H_2O$ were denoted as S-1, S-2, S-3, and S-4, respectively.

**2.4. Characterization.** The X-ray powder diffraction (XRD) pattern of the as-obtained samples was recorded on XD-3 (Beijing Purkinje General Instrument Co. Ltd.). The morphology and microstructures were analyzed by transmission electron microscope (TEM, JEOL JEM-2010) and field emission scanning electron microscopy (FESEM, JEOL JSM-7001F) equipped with energy dispersive X-ray spectroscopy (EDS, Oxford Instruments). The thermal stability of the Ni particles and Ni@$SnO_2$ is analyzed by thermogravimetric analysis (TGA, STA 409, Netzsch, Germany). TGA is performed on these samples from 25 to 800 °C with a heating rate of 10 °C/min in air flow. The specimen for microwave measurement was prepared by uniformly blending the Ni/$SnO_2$ absorbents with paraffin-wax in a mass fraction of 50 wt % and then being pressed into a ring-like compact structure (with a 3.04 mm inner diameter, 7.00 mm outer diameter). The relative complex permeability and permittivity of the Ni@$SnO_2$−paraffin composites were measured by a vector network analyzer (Agilent, N5244A) using the transmission/reflection method.

## 3. RESULTS AND DISCUSSION

The composition and phase of as-received products were characterized by X-ray diffraction (XRD). Figure 1a shows the

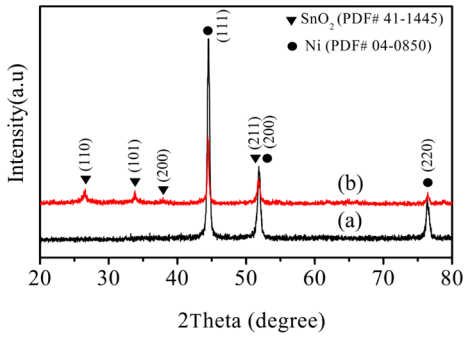


**Figure 1.** XRD patterns of (a) walnut-like Ni particles and (b) core-shell Ni/$SnO_2$ composite.

XRD profile of walnut-like Ni powders. The whole diffraction peaks could be well attributed to the face-centered cubic Ni (JCPDS card no. 04-0850). After adding HCl solution (0.1 M) and $SnCl_2·2H_2O$ (1 mmol) into hydrothermal system, the XRD pattern of final products was exhibited in Figure 1b. Besides the peaks associated with the Ni phase, the other peaks could match well with the tetragonal rutile $SnO_2$ (JCPDs no. 41-1445), which suggests that the composites are composed of Ni and $SnO_2$ (Figure 1b).

Figure 2a shows the morphology of as-obtained Ni submicron particles. It can be clearly observed that the as-synthesized Ni samples were comprised of monodispersed walnut-like spheres with a mean diameter of 500 nm. The overview morphology of Ni/$SnO_2$ composite is shown in Figure 2b. Obviously, the Ni particles were coated by a large number of nanoparticles to form a core-shell structured composite and the surface becomes rougher in comparison with raw Ni walnut spheres. Further observation from high magnification photographs of Ni/$SnO_2$ (Figure 2c,d), one can note that $SnO_2$ nanorods with the length of 30−50 nm and diameter of 10−20 nm were perpendicularly grown on the surface of nickel spheres and the average size of Ni/$SnO_2$ composite is about 600 nm. From FESEM images of nickel spheres and Ni/$SnO_2$ composites, it can draw the conclusion that a novel core−shell heterostructure ($SnO_2$ nanorods grown


DOI: 10.1021/acsami.5b05482
ACS Appl. Mater. Interfaces 2015, 7, 18815−18823

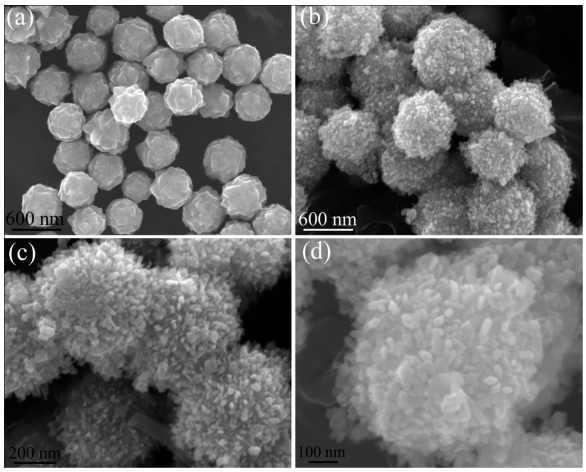


**Figure 2.** FESEM images of (a) Ni walnut spheres and (b–d) core-shell Ni/$SnO_2$ composites.

on Ni) was generated when HCl solution (0.1 M) and $SnCl_2 \cdot 2H_2O$ (1 mmol) were introduced into this reaction system.

To further uncover the composition of heterostructure, the EDS and elemental mappings were performed and the results were shown in Figure 3. From the EDS pattern (Figure 3b) of Ni/$SnO_2$ composite (mark in Figure 3a), it can be concluded the core-shell composites were made up of Ni, Sn, and O elements. The carbon element is also observed in the EDS profile. The C element is due to the rubberized fabric, which is utilized for pasting the sample. Pt peaks are also observed in the EDS profile because the SEM sample was prepared by sputtering of platinum onto the sample. The element mappings of Ni, Sn, and O are presented in Figure 3c–e, respectively. The elemental distribution is relatively uniform, which illustrates that the $SnO_2$ nanorods were uniformly grown on Ni particles.

Further detailed structural analysis of core–shell composites was analyzed by transmission electron microscopy (TEM) and high-resolution transmission electron microscopy (HRTEM). The TEM image in Figure 4a exhibits that the core-shell

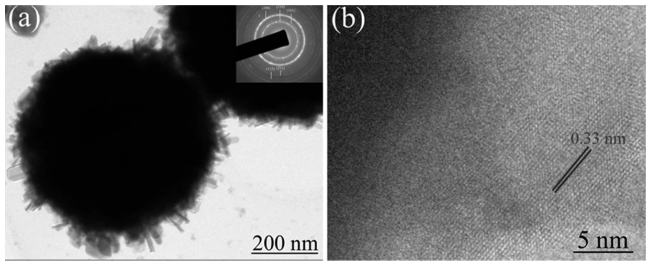


**Figure 4.** (a) TEM images of the as-prepared core-shell Ni/$SnO_2$ composites, selected area electron diffraction (SAED) pattern in rim region (inset) and (b) HRTEM of the nanorod in part a.

structured composite could be clearly observed from the obvious different contrast between Ni and $SnO_2$. Furthermore, close observation from Figure 4a, the core-shell heterostructures were composed of plentiful $SnO_2$ nanorods grown on the surface of Ni spheres, which coincided with FESEM observations. The corresponding selected-area electron diffraction (SAED) photograph (Figure 4a, inset) signifies that the $SnO_2$ nanorods are polycrystalline and the diffraction rings from inside to outside are in agreement with (110), (101), (200), (211), and (112) planes of rutile $SnO_2$, respectively. The lattice fringe spacing in HRTEM pattern was observed to be 0.33 nm (Figure 4b), which fitted well with the (110) planes of a tetragonal rutile structure of $SnO_2$.

The morphologies of Ni/$SnO_2$ composites were closely associated with the concentration of HCl in this reaction system. For the sake of investigating the relationship between morphology and concentration of HCl as well as mechanism

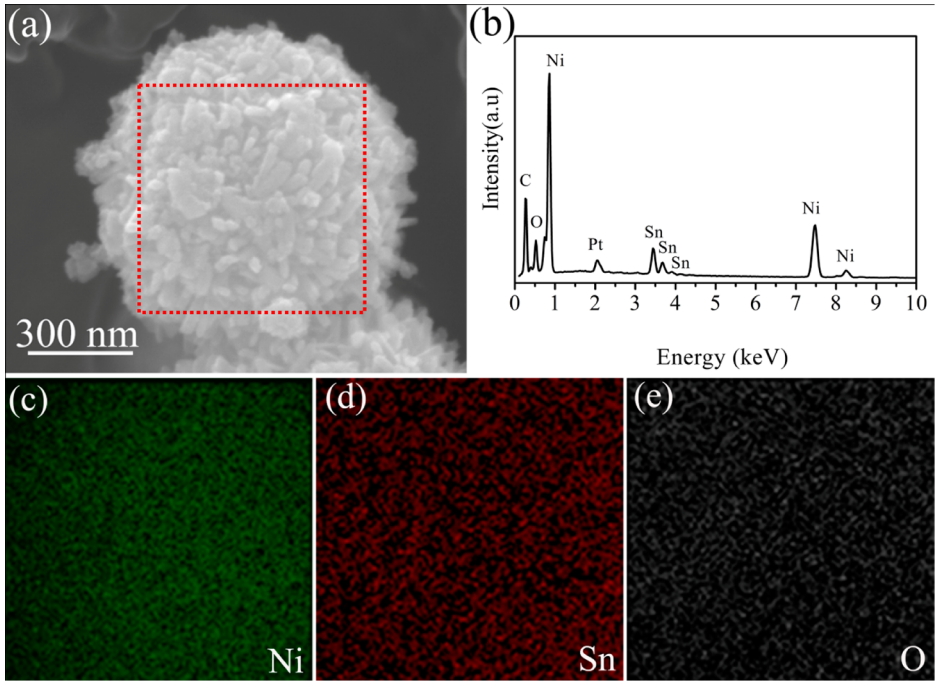


**Figure 3.** (a) FESEM image of an individual Ni/$SnO_2$ heterostructure, (b) EDS profile of Ni/$SnO_2$ composite and (c–e) corresponding elemental mappings of Ni, Sn, and O.


DOI: 10.1021/acsami.5b05482
ACS Appl. Mater. Interfaces 2015, 7, 18815–18823

formation of $SnO_2$ nanorods grown on the Ni composite, a series of experiments with different concentrations of HCl (0.05 M, 0.1 M, 0.4 M, 1.0 M) were carried out and the results were shown in Figure 5. From Figure 5a, it can be clearly

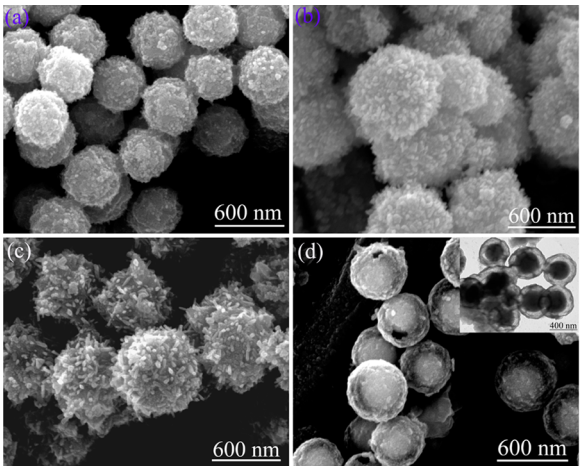


**Figure 5.** FESEM images of Ni/$SnO_2$ prepared at different concentrations of HCl: (a) 0.05 M, (b) 0.1 M, (c) 0.4 M, and (d) 1.0 M while other preparation concentrations remained constant. Inset of part d is the TEM image of Ni/$SnO_2$ prepared at 1.0 M HCl.

observed that the walnut-like Ni spheres were coated by dense plentiful $SnO_2$ nanoparticles at low concentration of HCl (0.05 M). The unique heterstructures of $SnO_2$ nanorods grown on Ni were obtained when the concentration of HCl is 0.1 M (Figure 5b), which is in accordance with the above observation (Figure 2). With increasing the concentration of HCl to 0.4 M, notably, the urchin-like Ni/$SnO_2$ were observed in Figure 5c. The thorn-like $SnO_2$ nanoparticles were grown on the Ni particles. Interestingly, further increasing the concentration of HCl to 1.0 M, combining Figure 5d and the inset, the novel core-void-shell structured Ni/$SnO_2$ can be obviously seen. The mechanism of such a structure is not clear and the related works are underway. In this protocol, HCl plays dual roles in forming $SnO_2$ nanorods grown on the Ni composite. On the one hand, the surfaces of the Ni walnut spheres were corroded by hydrochloric acid, which is beneficial for subsequent nucleation of $SnO_2$ nanoparticles. On the other hand, the $SnO_2$ nanoparticles were easily grown to $SnO_2$ nanorods with the assistance of an acid solution.[38,39] Too low of a concentration of hydrochloric acid, the $SnO_2$ nanparticles are produced on the surface of Ni particles instead of the nanorods. Too high a concentration of HCl induces suppression of the growth of $SnO_2$ nanoparticles, which also induce high corrosion of Ni. Finally, the voids between Ni and $SnO_2$ were generated. These results push us to draw a conclusion that the unique composite of $SnO_2$ nanorods grown on Ni particles can be obtained in the hydrochloric acid concentration range of 0.1−0.4 M. A plausible formation mechanism of core−shell $SnO_2$ nanorods/Ni sphere heterostructure was proposed based on hydrochloric acid concentration dependent experiments. As shown in Figure 6, first, the walnut-like Ni spheres were corroded by hydrochloric acid and $SnO_2$ nanoparticles were deposited on the corrosive Ni spheres.[40] Second, becasue of the acid conditions, the deposited $SnO_2$ nanoparticles are prone to growing into nanorods.[39]

Figure 7 shows the FESEM images of Ni/$SnO_2$ composites synthesized at various $SnCl_2{\cdot}2H_2O$ contents (0.5, 1.0, 1.5, and

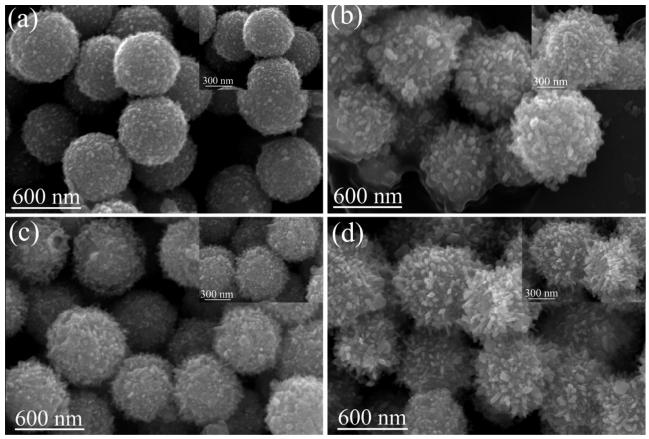


**Figure 7.** FESEM images of Ni/$SnO_2$ synthesized at various $SnCl_2{\cdot}2H_2O$ contents: (a) 0.5 mmol, (b) 1.0 mmol, (c) 1.5 mmol, and (d) 2.0 mmol while other synthesis parameters were kept constant. Insets are the corresponding high-magnification FESEM images.

2.0 mmol) while the other synthesis parameters are kept constant. At low $SnCl_2{\cdot}2H_2O$ contents (0.5 mmol), the final products (S-1) were composed of uniform dispersed composite spheres, in which the Ni spheres were densely covered by $SnO_2$ nanoparticles (Figure 7a). When the $SnCl_2{\cdot}2H_2O$ contents is 1.0 mmol (Figure 7b), the samples (S-2) exhibit the similar morphology with Figures 2−4). When the $SnCl_2{\cdot}2H_2O$ amounts are increased to 1.5 mmol, it is easily understand that the as-obtained products (S-3) show more dense and rodlike $SnO_2$-coated Ni particles (Figure 7c). With further increasing the $SnCl_2{\cdot}2H_2O$ contents to 2.0 mmol (S-4, Figure 7d), the diameter and length of $SnO_2$ nanorods grown on the surfaces of Ni spheres were bigger than those of products in Figure 7b. From the above analysis, the morphologies of $SnO_2$ nanorods, which are grown on the surfaces of Ni spheres, were crucially determined by the $SnCl_2{\cdot}2H_2O$ content.

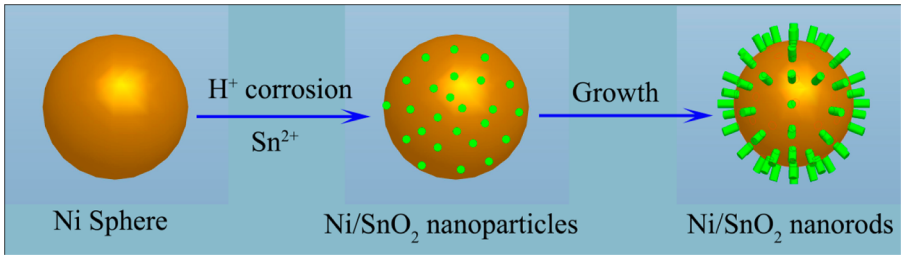


**Figure 6.** Plausible formation mechanism of core-shell Ni/$SnO_2$ composites with $SnO_2$ nanorods grown on Ni spheres.


DOI: 10.1021/acsami.5b05482
ACS Appl. Mater. Interfaces 2015, 7, 18815−18823

The Ni/$SnO_2$ composites prepared at different $SnCl_2{\cdot}2H_2O$ contents were further analyzed by the TEM instrument, and the results were shown in Figure 8 and Figure S1. From Figure 8

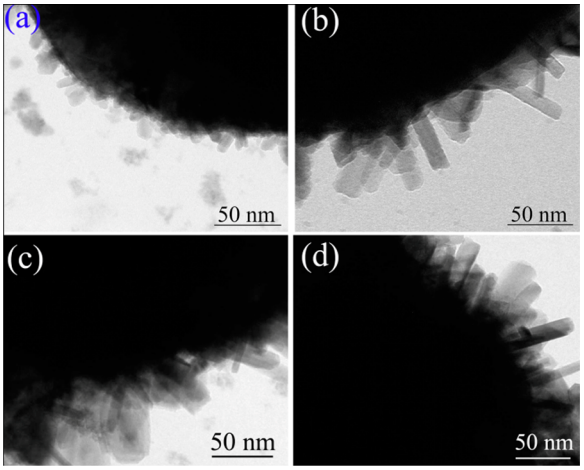


**Figure 8.** TEM images of Ni/$SnO_2$ composites prepared at different $SnCl_2{\cdot}2H_2O$ contents: (a) 0.5 mmol, (b) 1.0 mmol, (c) 1.5 mmol, and (d) 2.0 mmol while the other preparation parameters remained constant.

and Figure S1, notably, all the products obtained at different $SnCl_2{\cdot}2H_2O$ contents possess the core-shell structure through the different contrast between $SnO_2$ and Ni. The S-1 sample exhibits that the Ni cores are nearly coated by many $SnO_2$ nanoparticles with a mean diameter of 10 nm (Figure 8a). Figure 8b exhibits the morphology of products (S-2) obtained at 1.0 mmol of $SnCl_2{\cdot}2H_2O$. It can be noted that sparse $SnO_2$ nanorods with the length and size of about 40−50 and 10 nm were grown on the surfaces of Ni spheres. When 1.5 mmol of $SnCl_2{\cdot}2H_2O$ was introduced into this reaction system, the corroded Ni were covered by dense and bigger $SnO_2$ nanorods with a length and diameter of about 60 nm and 15−20 nm, respectively (Figure 8c). Furthermore, compared with Figure 8b, more dense and uniform $SnO_2$ nanorods grown on the corrosive Ni spheres can be observed as 2.0 mmol of $SnCl_2{\cdot}2H_2O$ was added into this reaction process. The length and diameter size of $SnO_2$ nanorods were about 70 and 20 nm (Figure 8d), respectively.

The electromagnetic wave absorption properties of a material are correlated with their relative complex permeability ($\mu_r = \mu' - j\mu''$) and permittivity ($\varepsilon_r = \varepsilon' - j\varepsilon''$).[41−43] The frequency dependence of complex permeability and permittivity of four core-shell Ni/$SnO_2$ composites are measured using a network analyzer. The real permittivity ($\varepsilon'$) and real permeability ($\mu'$) symbolize the storage ability of microwave energy, while the imaginary permittivity ($\varepsilon''$) and imaginary permeability ($\mu''$) represent dissipation ability of microwave energy.[1,16,44] Figure 9 shows the relative complex permeability and permittivity of the core-shell Ni/$SnO_2$ composites. It was noted that in the whole measured frequency range, $\varepsilon'$ values are nearly constant with little fluctuation (Figure 9a). Noticeably, the $\varepsilon'$ values of the S-2 sample are the highest among four core-shell Ni/$SnO_2$ samples, which suggests the more energy storage and polarization. Figure 9b presents the imaginary parts ($\varepsilon''$) of four core-shell Ni/$SnO_2$ composites. Notably, one can observe that the S-2 sample shows the largest $\varepsilon''$ values in the four samples, which indicates the superior dielectric loss. Interestingly, the four samples present the similar trend and multiple peaks on the $\varepsilon''$ values, indicating multiple resonances behavior. This resonance behavior is usually correlated with highly conductivity and skin effects,[45] electronic spin and charge polarizations owing to point effects, and polarized centers.[46] These phenomena are also clearly observed in our previous reports.[34,47−49] It mostly comes from the synergistic influence of walnut-like Ni spheres,

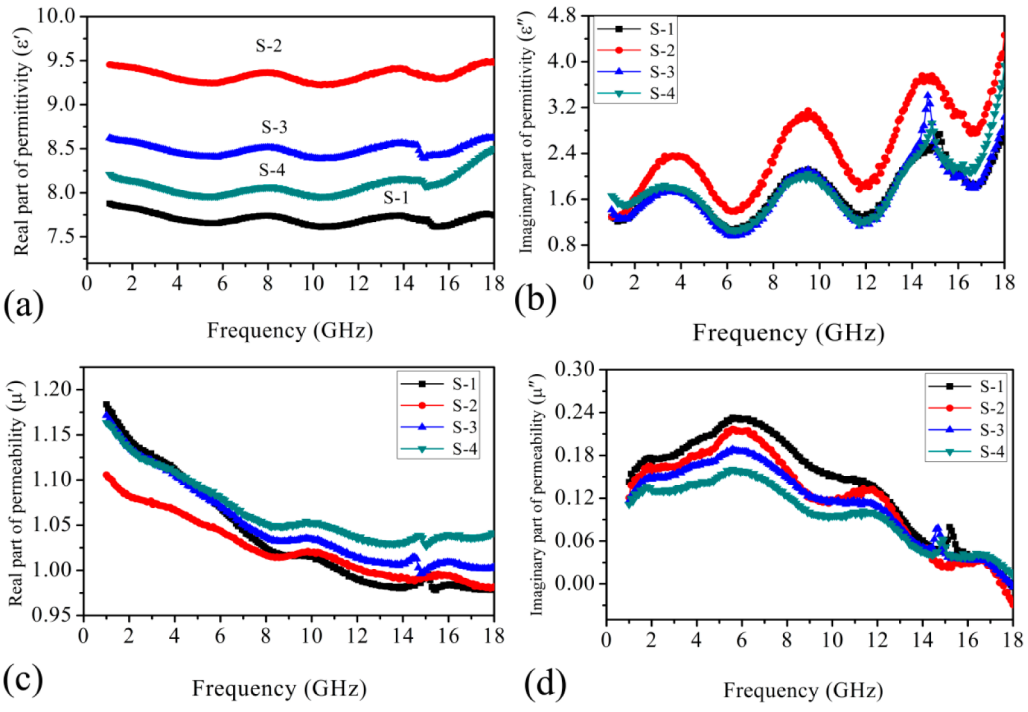


**Figure 9.** Frequency dependence of (a) the real part ($\varepsilon'$) and (b) imaginary part ($\varepsilon''$) of the complex permittivity, (c) the real part ($\mu'$) and (d) imaginary part ($\mu''$) of the complex permeability of four Ni/$SnO_2$ samples synthesized at different $SnCl_2{\cdot}2H_2O$ contents.


DOI: 10.1021/acsami.5b05482
ACS Appl. Mater. Interfaces 2015, 7, 18815−18823

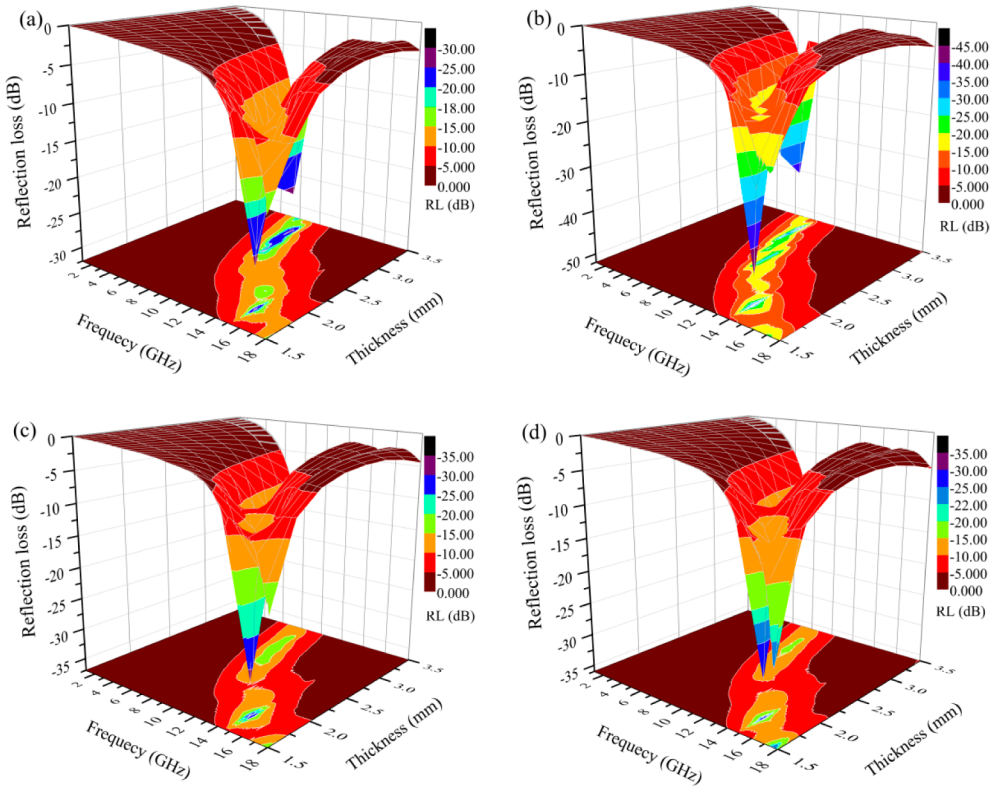


**Figure 10.** Frequency dependence of simulated reflection loss values of (a) S-1, (b) S-2, (c) S-3, and (d) S-4 samples with various thicknesses.

$SnO_2$ nanorods, and the interfaces between Ni and dielectric $SnO_2$ materials. The interfaces can induce additional interfacial polarizations,[50−53] which is beneficial for the dissipation of electromagnetic wave energy. Moreover, based on the free electron theory,[27,54] $\varepsilon'' \approx 1/\pi\varepsilon_0\rho f$, where $\rho$ is the resistivity. The conductivity of the S-2 samples is higher than those of other core-shell Ni/$SnO_2$ composite samples. For the S-2 sample, the sparse $SnO_2$ nanorods grown on Ni spheres can link with each other, and thus a discontinuous microcurrent gradually generates, which will induce high conductivity and cause conduction and electric loss.[55]

The real part ($\mu'$) and imaginary part ($\mu''$) values of core-shell Ni/$SnO_2$ are shown in Figure 9c,d. Four Ni/$SnO_2$ samples exhibit a similar decreased tendency with increasing the measured frequency (Figure 9c). While the $\mu''$ values first increase and then decrease with increasing frequency, it is noteworthy that the complex permeability of four Ni/$SnO_2$ composites shows the same trend (Figure 9d). The $\mu''$ presents the broad resonance peaks at 5−7 GHz, which is assigned to the natural resonance of nickel.[32] The other existence of resonance peaks are believed to be exchange resonances.[56−58] This novel heterostructures composed of $SnO_2$ nanorods grown on Ni spheres combining dielectric loss of $SnO_2$, magnetic loss of Ni, and interfacial polarization can possess enhanced electromagnetic wave absorption properties.

In general, the electromagnetic wave absorption properties of absorbers were evaluated by reflection loss (RL value of −10 dB means 90% of microwave absorption). The RL values of an absorbing material can be simulated based on the measured complex permittivity and permeability with a given absorber thickness using the transmit line theory by the following equation:[21,33,59,60]

$$RL = 20 \log_{10}|(Z_{in} - Z_0)/(Z_{in} + Z_0)| \quad (1)$$

$$Z_{in} = Z_0\sqrt{\frac{\mu_r}{\varepsilon_r}}\tanh\left(j\frac{2\pi f d\sqrt{\mu_r\varepsilon_r}}{c}\right) \quad (2)$$

in which $Z_0$ is the impedance of free space, $Z_{in}$ is the input characteristic impedance, $\varepsilon_r$ is the complex permittivity, $\mu_r$ is the complex permeability, $f$ is the frequency, $c$ is the velocity of light, and $d$ is the thickness of the Ni/$SnO_2$ composites. The calculated refection loss (RL) curves of the four Ni/$SnO_2$ composites with various thicknesses are shown in Figure 10. In the investigated region, the S-2 sample exhibits significantly enhanced electromagnetic wave absorption compared with the other three Ni/$SnO_2$ samples. The electromagnetic wave attenuation properties of the Ni/$SnO_2$ composites were dependent on the diameter and length of the $SnO_2$ nanorods. Too dense (Figure 8c,d) and small diameter (Figure 8a) of $SnO_2$ nanorods were harmful to microwave absorption, which is due to a poor impedance match caused by an unbalance of complex permittivity and permeability. The minimal RL of the S-2 sample is −45.0 dB at 13.9 GHz with the absorber thickness of only 1.8 mm (Figure 10b). The bandwidth (less than −10 dB) can be adjusted in the frequency of 6.0−18.0 GHz by adjusting the thickness to 1.5−3.5 mm. Compared with our earlier publications,[29,37] there are at least three advantages in this work. First, it is well-known that the microwave absorption properties were closely correlated with the microstructure of absorbers. By decreasing the size of metal Ni that would suppress the eddy current effect is favorable to the enhancement of microwave absorption properties. Moreover, the effect of the special rodlike $SnO_2$ shell on microwave absorption was also analyzed. Second, to evaluate the microwave absorption, it is not only based on the minimal


DOI: 10.1021/acsami.5b05482
ACS Appl. Mater. Interfaces 2015, 7, 18815−18823

reflection loss but some other factors, such as thickness and bandwidth should be also considered. In comparison with a $SnO_2$-coated Ni microsphere,[37] the $SnO_2$ nanorods grown on Ni composite shows the minimal reflection loss of −45.0 dB at 13.9 GHz with a thickness of only 1.8 mm, whereas the composite exhibits the minimal reflection loss of −42.8 dB at 9.8 GHz with a thickness of 3.0 mm. Furthermore, the bandwidth (RL less than −10 dB) of $SnO_2$ nanorods grown on Ni composite can reach 3.8 GHz (12.3−16.1 GHz) with an absorber thickness of 1.8 mm, which is superior to $SnO_2$-coated Ni microsphere composite with a bandwidth of 3.4 GHz (8.3−11.7 GHz) with a thickness of 3.0 mm. From these views, the $SnO_2$ nanorods grown on show the enhanced microwave absorption properties with the features of high efficiency absorption, thin thickness, and wide-band. Third, the unique one-dimensional $SnO_2$ rods can bring about an additional loss mechanism. The $SnO_2$ nanorods are supposed to be considered as an antenna receiver to allow more microwaves to enter the interior of the absorber. The discontinued microcurrent, which was caused when the $SnO_2$ nanorods were placed under the radiation of electromagnetic wave, can dissipate electromagnetic energy effectively. Notably, the reflection loss peaks gradually shifted to higher frequencies with decreasing absorber thickness, which could be well addressed by the geometrical effect.[24,61,62] As for the geometrical effect, it takes place when the reflected and incident waves in the absorbers are out of phase 180°, which is closely related to the thickness ($d$) of the absorbers. The relationship between $d_m$ and $f_m$ is given by the following equation $d_m = (nc/(4f_m(|\mu_r\varepsilon_r|)^{1/2}))$ ($n$ = 1, 3, 5,...). It can also deduce that the location of minimal peaks is inversely proportion to the absorber thickness.

In this heterostructure of $SnO_2$ nanorods grown on the surface of Ni spheres, $SnO_2$ nanorods play at least three roles in ameliorating electromagnetic wave absorption properties. First, introducing $SnO_2$ into this system can tune the complex permittivity of Ni/$SnO_2$ composites to improve the impedance match. Second, the core-shell structure between nickel and $SnO_2$ can cause additional space charge polarization and interfacial polarization, as shown in Figure 11, which is beneficial for enhancing microwave absorption. Third, the $SnO_2$ nanorods are supposed to be considered as an antenna receiver to allow more microwaves to enter the interior of the absorber.[55,63] The discontinues microcurrent, which was caused when $SnO_2$ nanorods were placed under the radiation of electromagnetic wave, can dissipate electromagnetic energy effectively.[51,64,65]

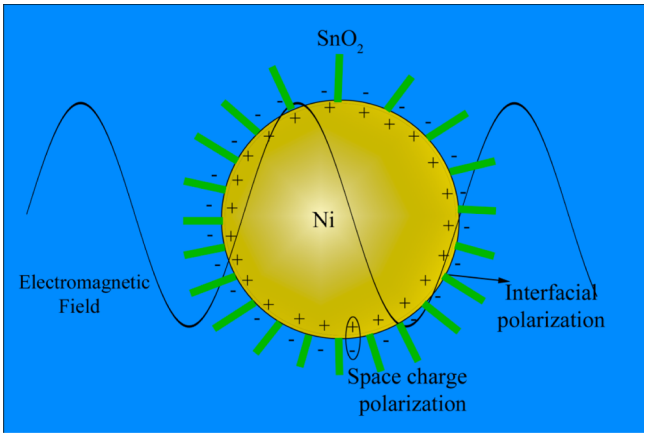


**Figure 11.** Schematic illustration of the interaction of electromagnetic waves with a core-shell dielectric-magnetic Ni sphere@$SnO_2$ nanorods composite.

To apply the electromagnetic wave absorbing materials in harsh conditions (such as high temperature), one important property of thermal stability should be considered.[66] Figure 12

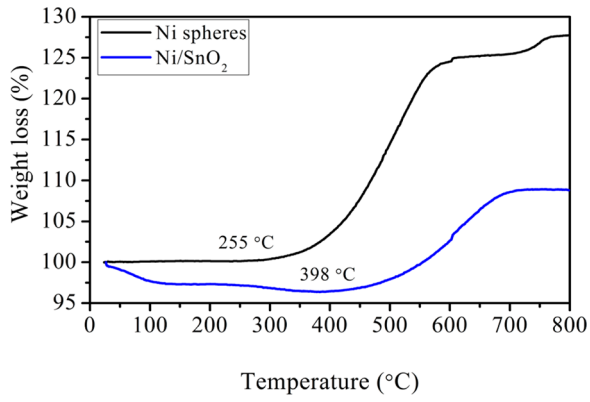


**Figure 12.** TGA curves of Ni spheres and core-shell structured Ni/$SnO_2$ (S-2) samples.

shows the thermal stability of Ni spheres and a core-shell composite (S-2) of $SnO_2$ nanorods grown on the Ni sphere. From Figure 12, both Ni spheres and Ni/$SnO_2$ composite exhibit a clear weight gain in the final stage because of the oxidation in air at increasing temperature. Notably, the weight of the Ni spheres starts to increase at ∼255 °C. After corrosion and growth of $SnO_2$ nanorods, the Ni spheres are protected and the oxidation temperature reaches to ∼398 °C. These results indicate the thermal stability of Ni/$SnO_2$ is superior to that of Ni spheres due to the presence of a protective $SnO_2$ nanorod shell.

## 4. CONCLUSION

In summary, $SnO_2$ nanorods grown on Ni novel core-shell composites were obtained via a facile two-step method. The morphology and microstructure of Ni/$SnO_2$ composites are crucially determined by the concentration of hydrochloric acid. Otherwise, on the basis of the hydrochloric acid concentration dependent experiments, a reasonable formation mechanism of such $SnO_2$ nanorods grown on Ni composites were proposed. The diameter and length of $SnO_2$ nanorods can be tailored by control of $SnCl_2{\cdot}2H_2O$. The electromagnetic absorption properties of the core-shell structured Ni/$SnO_2$ sample (S-2, $SnO_2$ nanorods with the diameter of 10 nm and length of about 40−50 nm) prepared with 1.0 mmol of $SnCl_2{\cdot}2H_2O$ exhibits excellent electromagnetic absorption. The optimal reflection loss (RL) is −45.0 dB at 13.9 GHz and RL less than −10 dB is 3.8 GHz (12.3−16.1 GHz) with only a thickness of 1.8 mm. This novel core-shell structured Ni-$SnO_2$ nanorods can be used as a promising electromagnetic wave absorber with the features of thin-thickness, high efficient absorption, and a wide-band.

## ■ ASSOCIATED CONTENT

### Supporting Information

The Supporting Information is available free of charge on the ACS Publications website at DOI: 10.1021/acsami.5b05482.

TEM images of Ni/$SnO_2$ composites (PDF)



DOI: 10.1021/acsami.5b05482
ACS Appl. Mater. Interfaces 2015, 7, 18815−18823

## AUTHOR INFORMATION


### Corresponding Authors

*E-mail: gang_shao@zzu.edu.cn.

*E-mail: zhangray@zzu.edu.cn. Phone: +86-371-60632007. Fax: +86-371-60632600.


### Notes

The authors declare no competing financial interest.

## ACKNOWLEDGMENTS

This work was sponsored by the financial support from the National Natural Science Foundation of China (Grant No. 51172213).

## REFERENCES


(1) Zhang, X.-J.; Wang, G.-S.; Cao, W.-Q.; Wei, Y.-Z.; Liang, J.-F.; Guo, L.; Cao, M.-S. Enhanced Microwave Absorption Property of Reduced Graphene Oxide (RGO)-$MnFe_2O_4$ Nanocomposites and Polyvinylidene Fluoride. *ACS Appl. Mater. Interfaces* **2014**, *6*, 7471−7478.

(2) Wang, H.; Wu, L.; Jiao, J.; Zhou, J.; Xu, Y.; Zhang, H.; Jiang, Z.; Shen, B.; Wang, Z. Covalent Interaction Enhanced Electromagnetic Wave Absorption in SiC/Co Hybrid Nanowires. *J. Mater. Chem. A* **2015**, *3*, 6517−6525.

(3) Chen, Y.-J.; Xiao, G.; Wang, T.-S.; Ouyang, Q.-Y.; Qi, L.-H.; Ma, Y.; Gao, P.; Zhu, C.-L.; Cao, M.-S.; Jin, H.-B. Porous $Fe_3O_4$/Carbon Core/Shell Nanorods: Synthesis and Electromagnetic Properties. *J. Phys. Chem. C* **2011**, *115*, 13603−13608.

(4) Saini, P.; Arora, M.; Gupta, G.; Gupta, B. K.; Singh, V. N.; Choudhary, V. High Permittivity Polyaniline-Barium Titanate Nanocomposites with Excellent Electromagnetic Interference Shielding Response. *Nanoscale* **2013**, *5*, 4330−4336.

(5) Liu, Y.; Liu, X.; Li, R.; Wen, W.; Wang, X. Design and Fabrication of Carbon Fiber/Carbonyl Iron Core-Shell Structure Composites as High-Performance Microwave Absorbers. *RSC Adv.* **2015**, *5*, 8713−8720.

(6) Liu, X.; Wu, N.; Cui, C.; Bi, N.; Sun, Y. One Pot Synthesis of $Fe_3O_4$/$MnO_2$ Core-Shell Structured Nanocomposites and Their Application as Microwave Absorbers. *RSC Adv.* **2015**, *5*, 24016−24022.

(7) Xie, S.; Guo, X.-N.; Jin, G.-Q.; Guo, X.-Y. Carbon Coated Co-SiC Nanocomposite with High-Performance Microwave Absorption. *Phys. Chem. Chem. Phys.* **2013**, *15*, 16104−16110.

(8) Liu, J.; Cheng, J.; Che, R.; Xu, J.; Liu, M.; Liu, Z. Double-Shelled Yolk−Shell Microspheres with $Fe_3O_4$ Cores and $SnO_2$ Double Shells as High-Performance Microwave Absorbers. *J. Phys. Chem. C* **2013**, *117*, 489−495.

(9) Wang, G.; Gao, Z.; Tang, S.; Chen, C.; Duan, F.; Zhao, S.; Lin, S.; Feng, Y.; Zhou, L.; Qin, Y. Microwave Absorption Properties of Carbon Nanocoils Coated with Highly Controlled Magnetic Materials by Atomic Layer Deposition. *ACS Nano* **2012**, *6*, 11009−11017.

(10) Cao, M.-S.; Yang, J.; Song, W.-L.; Zhang, D.-Q.; Wen, B.; Jin, H.-B.; Hou, Z.-L.; Yuan, J. Ferroferric Oxide/Multiwalled Carbon Nanotube vs Polyaniline/Ferroferric Oxide/Multiwalled Carbon Nanotube Multiheterostructures for Highly Effective Microwave Absorption. *ACS Appl. Mater. Interfaces* **2012**, *4*, 6949−6956.

(11) Zhang, Y.; Huang, Y.; Zhang, T.; Chang, H.; Xiao, P.; Chen, H.; Huang, Z.; Chen, Y. Broadband and Tunable High-Performance Microwave Absorption of an Ultralight and Highly Compressible Graphene Foam. *Adv. Mater.* **2015**, *27*, 2049−2053.

(12) Yu, Z.; Zhang, N.; Yao, Z.; Han, X.; Jiang, Z. Synthesis of Hierarchical Dendritic Micro-Nano Structure $Co_xFe_{1-x}$ Alloy with Tunable Electromagnetic Absorption Performance. *J. Mater. Chem. A* **2013**, *1*, 12462−12470.

(13) Yu, M.; Liang, C.; Liu, M.; Liu, X.; Yuan, K.; Cao, H.; Che, R. Yolk-Shell $Fe_3O_4$@$ZrO_2$ Prepared by a Tunable Polymer Surfactant Assisted Sol-Gel Method for High Temperature Stable Microwave Absorption. *J. Mater. Chem. C* **2014**, *2*, 7275−7283.

(14) Kong, L.; Yin, X.; Zhang, Y.; Yuan, X.; Li, Q.; Ye, F.; Cheng, L.; Zhang, L. Electromagnetic Wave Absorption Properties of Reduced Graphene Oxide Modified by Maghemite Colloidal Nanoparticle Clusters. *J. Phys. Chem. C* **2013**, *117*, 19701−19711.

(15) Zhu, Y.-F.; Zhang, L.; Natsuki, T.; Fu, Y.-Q.; Ni, Q.-Q. Facile Synthesis of $BaTiO_3$ Nanotubes and Their Microwave Absorption Properties. *ACS Appl. Mater. Interfaces* **2012**, *4*, 2101−2106.

(16) Wang, L.; Jia, X.; Li, Y.; Yang, F.; Zhang, L.; Liu, L.; Ren, X.; Yang, H. Synthesis and Microwave Absorption Property of Flexible Magnetic Film Based on Graphene Oxide/Carbon Nanotubes and $Fe_3O_4$ Nanoparticles. *J. Mater. Chem. A* **2014**, *2*, 14940−14946.

(17) Guo, J.; Wu, H.; Liao, X.; Shi, B. Facile Synthesis of Size-Controlled Silver Nanoparticles Using Plant Tannin Grafted Collagen Fiber As Reductant and Stabilizer for Microwave Absorption Application in the Whole Ku Band. *J. Phys. Chem. C* **2011**, *115*, 23688−23694.

(18) Dhawan, R.; Kumari, S.; Kumar, R.; Dhawan, S. K.; Dhakate, S. R. Mesocarbon Microsphere Composites with $Fe_3O_4$ Nanoparticles for Outstanding Electromagnetic Interference Shielding Effectiveness. *RSC Adv.* **2015**, *5*, 43279−43289.

(19) Xiang, J.; Li, J.; Zhang, X.; Ye, Q.; Xu, J.; Shen, X. Magnetic Carbon Nanofibers Containing Uniformly Dispersed Fe/Co/Ni Nanoparticles as Stable and High-Performance Electromagnetic Wave Absorbers. *J. Mater. Chem. A* **2014**, *2*, 16905−16914.

(20) Yang, Z.; Li, Z.; Yu, L.; Yang, Y.; Xu, Z. Achieving High Performance Electromagnetic Wave Attenuation: a Rational Design of Silica Coated Mesoporous Iron Microcubes. *J. Mater. Chem. C* **2014**, *2*, 7583−7588.

(21) Wang, Z.; Wu, L.; Zhou, J.; Cai, W.; Shen, B.; Jiang, Z. Magnetite Nanocrystals on Multiwalled Carbon Nanotubes as a Synergistic Microwave Absorber. *J. Phys. Chem. C* **2013**, *117*, 5446−5452.

(22) Liang, C.; Liu, C.; Wang, H.; Wu, L.; Jiang, Z.; Xu, Y.; Shen, B.; Wang, Z. SiC-$Fe_3O_4$ Dielectric-Magnetic Hybrid Nanowires: Controllable Fabrication, Characterization and Electromagnetic Wave Absorption. *J. Mater. Chem. A* **2014**, *2*, 16397−16402.

(23) Guo, H.; Zhan, Y.; Chen, Z.; Meng, F.; Wei, J.; Liu, X. Decoration of Basalt Fibers with Hybrid $Fe_3O_4$ Microspheres and Their Microwave Absorption Application in Bisphthalonitrile Composites. *J. Mater. Chem. A* **2013**, *1*, 2286−2296.

(24) Tong, G.; Liu, F.; Wu, W.; Du, F.; Guan, J. Rambutan-Like Ni/MWCNT Heterostructures: Easy Synthesis, Formation Mechanism, and Controlled Static Magnetic and Microwave Electromagnetic Characteristics. *J. Mater. Chem. A* **2014**, *2*, 7373−7382.

(25) Guo, J.; Wang, X.; Miao, P.; Liao, X.; Zhang, W.; Shi, B. One-Step Seeding Growth of Controllable Ag@ Ni Core−Shell Nanoparticles on Skin Collagen Fiber with Introduction of Plant Tannin and Their Application in High-Performance Microwave Absorption. *J. Mater. Chem.* **2012**, *22*, 11933−11942.

(26) Wang, G.; Peng, X.; Yu, L.; Wan, G.; Lin, S.; Qin, Y. Enhanced Microwave Absorption of ZnO Coated with Ni Nanoparticles Produced by Atomic Layer Deposition. *J. Mater. Chem. A* **2015**, *3*, 2734−2740.

(27) Xu, P.; Han, X.; Wang, C.; Zhou, D.; Lv, Z.; Wen, A.; Wang, X.; Zhang, B. Synthesis of Electromagnetic Functionalized Nickel/Polypyrrole Core/Shell Composites. *J. Phys. Chem. B* **2008**, *112*, 10443−10448.

(28) Zhao, B.; Shao, G.; Fan, B.; Zhao, W.; Zhang, R. Fabrication and Enhanced Microwave Absorption Properties of $Al_2O_3$ Nanoflake-Coated Ni Core-Shell Composite Microspheres. *RSC Adv.* **2014**, *4*, 57424−57429.

(29) Zhao, B.; Shao, G.; Fan, B.; Li, W.; Pian, X.; Zhang, R. Enhanced Electromagnetic Wave Absorption Properties of Ni−$SnO_2$ Core−Shell Composites Synthesized by a Simple Hydrothermal Method. *Mater. Lett.* **2014**, *121*, 118−121.

(30) Li, W.; Qiu, T.; Wang, L.; Ren, S.; Zhang, J.; He, L.; Li, X. Preparation and Electromagnetic Properties of Core/Shell Polystyrene@Polypyrrole@Nickel Composite Microspheres. *ACS Appl. Mater. Interfaces* **2013**, *5*, 883−891.




DOI: 10.1021/acsami.5b05482
*ACS Appl. Mater. Interfaces* 2015, 7, 18815−18823

(31) Dong, X.; Zhang, X.; Huang, H.; Zuo, F. Enhanced Microwave Absorption in Ni/Polyaniline Nanocomposites by Dual Dielectric Relaxations. *Appl. Phys. Lett.* **2008**, *92*, 013127.
(32) Chen, T.; Deng, F.; Zhu, J.; Chen, C.; Sun, G.; Ma, S.; Yang, X. Hexagonal and Cubic Ni Nanocrystals Grown on Graphene: Phase-Controlled Synthesis, Characterization and Their Enhanced Microwave Absorption Properties. *J. Mater. Chem.* **2012**, *22*, 15190−15197.
(33) Zhao, B.; Shao, G.; Fan, B.; Zhao, W.; Zhang, R. Investigation of the Electromagnetic Absorption Properties of Ni@$TiO_2$ and Ni@$SiO_2$ Composite Microspheres with Core-Shell Structure. *Phys. Chem. Chem. Phys.* **2015**, *17*, 2531−2539.
(34) Zhao, B.; Shao, G.; Fan, B.; Zhao, W.; Chen, Y.; Zhang, R. Facile Synthesis of Crumpled ZnS Net-Wrapped Ni Walnut Spheres with Enhanced Microwave Absorption Properties. *RSC Adv.* **2015**, *5*, 9806−9814.
(35) Liu, X.; Feng, C.; Or, S. W.; Sun, Y.; Jin, C.; Li, W.; Lv, Y. Investigation on Microwave Absorption Properties of CuO/$Cu_2O$-Coated Ni Nanocapsules as Wide-Band Microwave Absorbers. *RSC Adv.* **2013**, *3*, 14590−14594.
(36) Li, N.; Cao, M.; Hu, C. A Simple Approach to Spherical Nickel-Carbon Monoliths as Light-Weight Microwave Absorbers. *J. Mater. Chem.* **2012**, *22*, 18426−18432.
(37) Zhao, B.; Shao, G.; Fan, B.; Guo, W.; Chen, Y.; Zhang, R. Preparation of $SnO_2$-Coated Ni Microsphere Composites with Controlled Microwave Absorption Properties. *Appl. Surf. Sci.* **2015**, *332*, 112−120.
(38) Wang, H.; Rogach, A. L. Hierarchical $SnO_2$ Nanostructures: Recent Advances in Design, Synthesis, and Applications. *Chem. Mater.* **2014**, *26*, 123−133.
(39) Vayssieres, L.; Graetzel, M. Highly Ordered $SnO_2$ Nanorod Arrays from Controlled Aqueous Growth. *Angew. Chem.* **2004**, *116*, 3752−3756.
(40) Wang, A.; Wang, W.; Long, C.; Li, W.; Guan, J.; Gu, H.; Xu, G. Facile Preparation, Formation Mechanism and Microwave Absorption Properties of Porous Carbonyl Iron Flakes. *J. Mater. Chem. C* **2014**, *2*, 3769−3776.
(41) Du, Y.; Liu, W.; Qiang, R.; Wang, Y.; Han, X.; Ma, J.; Xu, P. Shell Thickness-Dependent Microwave Absorption of Core−Shell $Fe_3O_4$@C Composites. *ACS Appl. Mater. Interfaces* **2014**, *6*, 12997−13006.
(42) Sun, G.; Dong, B.; Cao, M.; Wei, B.; Hu, C. Hierarchical Dendrite-Like Magnetic Materials of $Fe_3O_4$, $\gamma$-$Fe_2O_3$, and Fe with High Performance of Microwave Absorption. *Chem. Mater.* **2011**, *23*, 1587−1593.
(43) Ren, Y.; Zhu, C.; Zhang, S.; Li, C.; Chen, Y.; Gao, P.; Yang, P.; Ouyang, Q. Three-Dimensional $SiO_2$@$Fe_3O_4$ Core/Shell Nanorod Array/Graphene Architecture: Synthesis and Electromagnetic Absorption Properties. *Nanoscale* **2013**, *5*, 12296−12303.
(44) Zhou, W.; Hu, X.; Bai, X.; Zhou, S.; Sun, C.; Yan, J.; Chen, P. Synthesis and Electromagnetic, Microwave Absorbing Properties of Core−Shell $Fe_3O_4$−Poly(3, 4-ethylenedioxythiophene) Microspheres. *ACS Appl. Mater. Interfaces* **2011**, *3*, 3839−3845.
(45) Li, H.; Huang, Y.; Sun, G.; Yan, X.; Yang, Y.; Wang, J.; Zhang, Y. Directed Growth and Microwave Absorption Property of Crossed ZnO Netlike Micro-/Nanostructures. *J. Phys. Chem. C* **2010**, *114*, 10088−10091.
(46) Watts, P. C. P.; Hsu, W. K.; Barnes, A.; Chambers, B. High Permittivity from Defective Multiwalled Carbon Nanotubes in the X-Band. *Adv. Mater.* **2003**, *15*, 600−603.
(47) Zhao, B.; Shao, G.; Fan, B.; Wang, C.; Xie, Y.; Zhang, R. Preparation and Enhanced Microwave Absorption Properties of Ni Microspheres Coated with $Sn_6O_4(OH)_4$ Nanoshells. *Powder Technol.* **2015**, *270*, 20−26.
(48) Zhao, B.; Shao, G.; Fan, B.; Zhao, W.; Xie, Y.; Zhang, R. ZnS Nanowall Coated Ni Composites: Facile Preparation and Enhanced Electromagnetic Wave Absorption. *RSC Adv.* **2014**, *4*, 61219−61225.
(49) Zhao, B.; Shao, G.; Fan, B.; Zhao, W.; Zhang, R. Facile Synthesis and Enhanced Microwave Absorption Properties of Novel Hierarchical Heterostructures Based on a Ni Microsphere-CuO Nano-Rice Core-Shell Composite. *Phys. Chem. Chem. Phys.* **2015**, *17*, 6044−6052.
(50) Yang, H.-J.; Cao, W.-Q.; Zhang, D.-Q.; Su, T.-J.; Shi, H.-L.; Wang, W.-Z.; Yuan, J.; Cao, M.-S. NiO Hierarchical Nanorings on SiC: Enhancing Relaxation to Tune Microwave Absorption at Elevated Temperature. *ACS Appl. Mater. Interfaces* **2015**, *7*, 7073−7077.
(51) Zhao, B.; Shao, G.; Fan, B.; Zhao, W.; Xie, Y.; Zhang, R. Synthesis of Flower-Like CuS Hollow Microspheres Based on Nanoflakes Self-Assembly and Their Microwave Absorption Properties. *J. Mater. Chem. A* **2015**, *3*, 10345−10352.
(52) Liu, Q.; Zhang, D.; Fan, T. Electromagnetic Wave Absorption Properties of Porous Carbon/Co Nanocomposites. *Appl. Phys. Lett.* **2008**, *93*, 013110.
(53) Han, M.; Yin, X.; Kong, L.; Li, M.; Duan, W.; Zhang, L.; Cheng, L. Graphene-Wrapped ZnO Hollow Spheres with Enhanced Electromagnetic Wave Absorption Properties. *J. Mater. Chem. A* **2014**, *2*, 16403−16409.
(54) Liu, X.; Geng, D.; Meng, H.; Shang, P.; Zhang, Z. Microwave-Absorption Properties of ZnO-Coated Iron Nanocapsules. *Appl. Phys. Lett.* **2008**, *92*, 173117.
(55) Tong, G.; Yuan, J.; Wu, W.; Hu, Q.; Qian, H.; Li, L.; Shen, J. Flower-Like Co Superstructures: Morphology and Phase Evolution Mechanism and Novel Microwave Electromagnetic Characteristics. *CrystEngComm* **2012**, *14*, 2071−2079.
(56) Aharoni, A. Exchange Resonance Modes in a Ferromagnetic Sphere. *J. Appl. Phys.* **1991**, *69*, 7762−7764.
(57) Toneguzzo, P.; Acher, O.; Viau, G.; Fiévet-Vincent, F.; Fiévet, F. Observations of Exchange Resonance Modes on Submicrometer Sized Ferromagnetic Particles. *J. Appl. Phys.* **1997**, *81*, 5546−5548.
(58) Liu, T.; Zhou, P.; Xie, J.; Deng, L. Electromagnetic and Absorption Properties of Urchinlike Ni Composites at Microwave Frequencies. *J. Appl. Phys.* **2012**, *111*, 093905.
(59) Pan, G.; Zhu, J.; Ma, S.; Sun, G.; Yang, X. Enhancing the Electromagnetic Performance of Co through the Phase-Controlled Synthesis of Hexagonal and Cubic Co Nanocrystals Grown on Graphene. *ACS Appl. Mater. Interfaces* **2013**, *5*, 12716−12724.
(60) Chen, X.; Meng, F.; Zhou, Z.; Tian, X.; Shan, L.; Zhu, S.; Xu, X.; Jiang, M.; Wang, L.; Hui, D.; Wang, Y.; Lu, J.; Gou, J. One-Step Synthesis of Graphene/Polyaniline Hybrids by in Situ Intercalation Polymerization and Their Electromagnetic Properties. *Nanoscale* **2014**, *6*, 8140−8148.
(61) Wang, C.; Han, X.; Zhang, X.; Hu, S.; Zhang, T.; Wang, J.; Du, Y.; Wang, X.; Xu, P. Controlled Synthesis and Morphology-Dependent Electromagnetic Properties of Hierarchical Cobalt Assemblies. *J. Phys. Chem. C* **2010**, *114*, 14826−14830.
(62) Wang, Q.; Lei, Z.; Chen, Y.; Ouyang, Q.; Gao, P.; Qi, L.; Zhu, C.; Zhang, J. Branched Polyaniline/Molybdenum Oxide Organic/Inorganic Heteronanostructures: Synthesis and Electromagnetic Absorption Properties. *J. Mater. Chem. A* **2013**, *1*, 11795−11801.
(63) Zhuo, R. F.; Feng, H. T.; Liang, Q.; Liu, J. Z.; Chen, J. T.; Yan, D.; Feng, J. J.; Li, H. J.; Cheng, S.; Geng, B. S.; Xu, X. Y.; Wang, J.; Wu, Z. G.; Yan, P. X.; Yue, G. H. Morphology-Controlled Synthesis, Growth Mechanism, Optical and Microwave Absorption Properties of ZnO Nanocombs. *J. Phys. D: Appl. Phys.* **2008**, *41*, 185405.
(64) Zhao, B.; Shao, G.; Fan, B.; Xie, Y.; Zhang, R. Preparation and Electromagnetic Wave Absorption of Chain-Like CoNi by a Hydrothermal Route. *J. Magn. Magn. Mater.* **2014**, *372*, 195−200.
(65) Wang, G.-S.; Nie, L.-Z.; Yu, S.-H. Tunable Wave Absorption Properties of $\beta$-$MnO_2$ Nanorods and Their Application in Dielectric Composites. *RSC Adv.* **2012**, *2*, 6216−6221.
(66) Zhu, J.; Wei, S.; Haldolaarachchige, N.; Young, D. P.; Guo, Z. Electromagnetic Field Shielding Polyurethane Nanocomposites Reinforced with Core−Shell Fe−Silica Nanoparticles. *J. Phys. Chem. C* **2011**, *115*, 15304−15310.


DOI: 10.1021/acsami.5b05482
*ACS Appl. Mater. Interfaces* 2015, 7, 18815−18823